SPH Modelling of the Impact of a Flat Plate upon an Aerated Water Surface

Hassan Sdiq, David I. Graham, Jason Hughes*
School of Computing, Electronics and Mathematics, Plymouth University, UK

ABSTRACT

Smoothed particle hydrodynamics (SPH) is a particle-based numerical method that is well-suited to fluid flow problems where the computational domain becomes highly deformed. In this paper we use an SPH method to simulate the impact of a flat plate on a water surface, as carried out experimentally in the FROTH project at Plymouth University, Ma et al. (2016). A novel feature of the experiments was that, in order to mimic wave/structure impacts, the water was aerated by bubbling air from underneath the water surface. This created a non-homogeneous, compressible mixture. This implies that, for good quality simulations, very large numbers of particles are required, meaning in turn that parallelised code is required. Simulations have been carried out using single-phase SPH models, in both two and three spatial dimensions. The speed of the plate as it enters the water is specified from the experiments and data from this are used as boundary conditions for the SPH model. The results show generally good agreement in terms of free surface shape, pressure distributions, sound wave developments/reaction and pressure/time traces, but we note that maximum pressures as well as propagation and reaction of sound waves are highly dependent upon the sound speed specified within the weakly-compressible SPH model.

KEY WORDS: SPH modelling, solid fluid interaction, aerated water, free surface flow.

INTRODUCTION

Smoothed particle hydrodynamic (SPH) has previously been successfully applied to the modelling of fluid flow, solid mechanics and fluid-solid interactions, especially when this involves large deformations. SPH is a fully Lagrangian method, which does not require the use of any mesh. It was invented by Lucy (1977) and Gingold & Monaghan (1977). Since then, the use of SPH has expanded in many areas of solid and fluid dynamics. Nowadays, the SPH method is widely used to simulate flows in hydro-engineering and geophysical applications.

In the Weakly Compressible Smoothed Particle Hydrodynamics (WCSPH) method, fluid pressure is related to particle density using a stiff equation of state. In the present work, WCSPH is discussed and used to simulate dropping a flat plate in to still water. The WCSPH method allows density fluctuations of around one percent by using a numerical speed of sound which is normally taken as ten times higher than the maximum fluid velocity.

GOVERNING EQUATIONS

In smoothed particle hydrodynamics (SPH), the equations of conservation of momentum and mass are

$$\frac{D\boldsymbol{u}}{Dt} = -\frac{1}{\rho}\nabla p + \upsilon\nabla^2\boldsymbol{u} + \boldsymbol{g}, \tag{1}$$

$$\frac{D\rho}{Dt} = -\rho\nabla.\boldsymbol{u}. \tag{2}$$

where a vector quantity is represented in bold face. In these equations, $\boldsymbol{u}$ is the velocity, t is the time, ρ is the density, p is the pressure, $\boldsymbol{g}$ is the gravitational acceleration and υ is the kinematic viscosity. The general idea of SPH is to approximate these equations by representing the continuous fluid as a set of discrete particles.

SPH Methodology

In SPH, the fluid is represented as a set of discrete particles, with each particle carrying its own mass, density, velocity and pressure. In SPH, a function f is approximated by the following:

$$f(\boldsymbol{x}_i) = \sum_j V_j f_j W_{ij}, \tag{3}$$

where $W_{ij} = W(|\boldsymbol{x}_i - \boldsymbol{x}_j|, h)$ is the smoothing function, h is the smoothing length and V_j is the particle volume (which can be written as $V_j = \frac{\boldsymbol{m_j}}{\rho_j}$). A similar process can be applied to obtain the derivative of function f

$$\nabla f(\boldsymbol{x}_i) = \sum_j \frac{m_j}{\rho_j} f(\boldsymbol{x}_j)\nabla_i W_{ij}, \tag{4}$$

where $\nabla_i W_{ij} = \nabla W(|\boldsymbol{x}_i - \boldsymbol{x}_j|, h)$ and the subscript j denotes the neighbouring particles which are located in the support domain.

Kernel function

The Kernel function influences the results of SPH approximations. The use of a high-order kernel is advisable to capture the complex flow phenomena. In this work the Wendland kernel, Wendland (1995), will be

used, due to it being more suitable for MPI code and avoids the need for any 'tensile correction':

$$w(q) = \alpha_d \begin{cases} (1-\frac{q}{2})^4(2q+1), & \text{for} \quad 0 \le q \le 2 \\ 0 & \text{for} \quad q \ge 2 \end{cases}$$

where $q = r/h$ and $\alpha_d = 7/(4\pi h^2)$ and $\alpha_d = 7/(8\pi h^3)$ for 2D and 3D, respectively.

Continuity equation

The conservation of mass is characterised by the equation

$$\frac{\partial \rho}{\partial t} + \nabla.(\rho \boldsymbol{u}) = \frac{\partial \rho}{\partial t} + \boldsymbol{u}.\nabla\rho + \rho.\nabla\boldsymbol{u} = 0,$$

i.e

$$\frac{D\rho}{Dt} = -\rho\nabla\boldsymbol{u},$$

where

$$\frac{D}{Dt} = \frac{\partial}{\partial t} + \boldsymbol{u}.\nabla$$

is the convective direction (following particle).
Using

$$-\rho\nabla\boldsymbol{u} = -\nabla.(\rho\boldsymbol{u}) + \boldsymbol{u}.\nabla\rho,$$

we get

$$\frac{D\rho_i}{Dt} = -\nabla_i.(\rho_i\boldsymbol{u}_i) + \boldsymbol{u}_i.\nabla_i\rho_i \tag{5}$$

Applying the SPH approximation Eq.4 into equation Eq.5,

$$\frac{D\rho_i}{Dt} = -\sum_j \frac{m_j}{\rho_j}(\rho_j\boldsymbol{u}_j).\nabla_i W_{ij} + \boldsymbol{u}_i \sum_j \frac{m_j}{\rho_j}\rho_j.\nabla_i W_{ij}.$$

After simplifying, this becomes

$$\frac{d\rho_i}{dt} = \sum_j m_j(\boldsymbol{u}_i - \boldsymbol{u}_j).\nabla_i W_{ij}.$$

Acceleration

Based on the SPH approximations shown in Eqs. 3 and 4, the pressure gradient in the governing equation 1 can be written in SPH form as

$$\nabla p_i = \sum_j m_j \frac{p_i}{\rho_j}\nabla_i W_{ij}. \tag{6}$$

The product rule for differentiation gives us the equation

$$\nabla(p1) = 1\nabla p + p\nabla 1 \longrightarrow 1\nabla p = \nabla(p1) - p\nabla 1,$$

which can be used to reformulate the pressure force term as

$$\nabla p_i = \sum_j \frac{m_j}{\rho_j} p_j \nabla_i W ij + p_i \sum_j \frac{m_j}{\rho_j} 1\nabla_i W_{ij} \tag{7}$$

which, from Eq.(7) after simplification becomes

$$\nabla p_i = \sum_j \frac{m_j}{\rho_j}(p_j + p_i)\nabla_i W_{ij}. \tag{8}$$

From Eq.(2), we have

$$\frac{d\boldsymbol{u}_i}{dt} = \boldsymbol{g}_i - \sum_j \frac{m_j}{\rho_i\rho_j}(p_i + p_j)\nabla_i W_{ij} + \nu\nabla^2 u \tag{9}$$

Now the particle approximation of the full Navier-Stokes equation, including viscosity term, is given as

$$\frac{D\boldsymbol{u}_i}{Dt} = \boldsymbol{g}_i - \sum_j \frac{m_j}{\rho_i\rho_j}(p_i + p_j + \Pi_{ij})\nabla_i W_{ij} \tag{10}$$

where Π_{ij} is a viscous term and $\boldsymbol{g}_i$ is the gravitational acceleration. Following Morris et al. (1997) we use

$$\Pi_{ij} = m_j \frac{(\mu_i + \mu_j)(\boldsymbol{x}_i - \boldsymbol{x}_j)}{\rho_i\rho_j}.\boldsymbol{u}_{ij} \tag{11}$$

where $\mu_j = \rho_j\nu_j$ and ν_j is the kinematic viscosity. In the calculations we use the physical viscosity of water i.e. 0.001 Pa.s.

Pressure Evaluation

After updating the density for each particle, we need to update the pressure p. The pressure can be evaluated with a stiff equation of state, Monaghan (1994). The equation of state used is:

$$p(\rho) = \frac{c_0^2\rho_0}{\gamma}[(\frac{\rho}{\rho_0})^\gamma - 1], \tag{12}$$

where c_0 is the reference speed of sound, $\rho_0 = 1000kg/m^3$, c_0 is chosen as at least ten times the maximum fluid velocity u, γ is constant and a value of 7 is employed for water, Monaghan (1994).

The sound speeds used in this study are much larger than ten times the maximum fluid velocity u and are set as physical sound speeds determined by the aeration level in the water-air mixture. Figure 1 illustrates the speed of sound in a water-air mixture. We use the following equation,

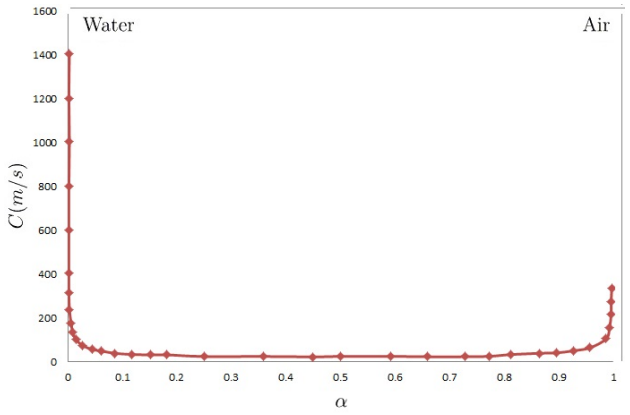

Fig. 1 The speed of sound in water-air mixture at one atmospheric pressure and 15 C. c is speed of sound, α is volume fraction, Brennen (1995)

Brennen (1995), to find the speed of sound at different aeration levels:

$$\frac{1}{c^2} = \frac{\alpha}{kp}(\rho_l(1-\alpha) + \rho_g\alpha), \tag{13}$$

where c is speed of sound, α is the aeration level, ρ_l and ρ_g are the densities of fluid and air, respectively. k is constant and is taken as 1. For pure water, we use speed of sound 350 m/s which was the maximum possible speed of sound that would give stable simulations. From equation 13, the speed of sound used for aerated levels of 0.78%, 1.02% and 1.6% were 122 m/s , 107 m/s and 86 m/s, respectively.

Density re-initialization

In this study we use the Shepard filter (see Panizzo & Dalrymple (2004)), which is used to reduce pressure oscillations due to density variations. The Shepard method is a quick and simple correction to the density, and the following procedure is applied:

$$\rho_i^{new} = \sum_j \rho_j \widetilde{W_{ij}} \frac{m_j}{\rho_j} = \sum_j m_j \widetilde{W_{ij}}, \tag{14}$$

where the kernel has been corrected using a zeroth-order correction

$$\widetilde{W}_{ij} = \frac{W_{ij}}{\sum_j \widetilde{W_{ij}} \frac{m_j}{\rho_j}}. \tag{15}$$

The Shepard filter is applied every 10 time steps. We also carried out some calculations applying the Shepard filter every 5 or 20 time steps and here was very little difference in the simulations.

Boundary Conditions

In SPH the kernel is truncated near the boundaries (see Figure 2) and to complete the kernel in this region and to prevent the escape of fluid particles from the domain, introducing a set of particles on the boundary with some conditions is required.

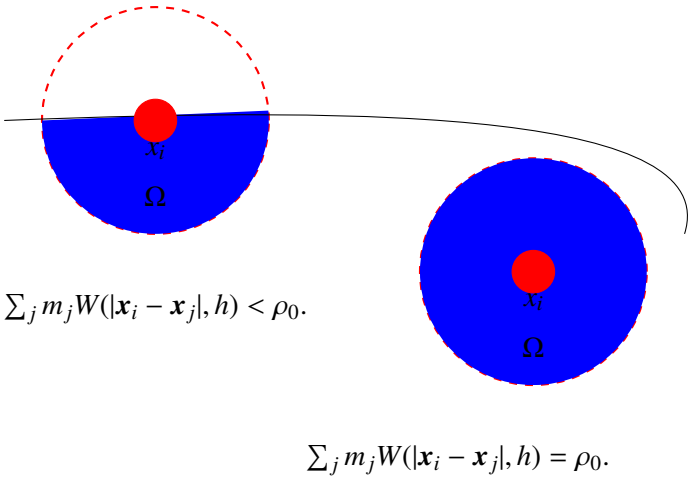

Fig. 2 Configurations of the kernel support domain inside the fluid and near the boundary.

There are four main treatments which have been introduced in the literature and are widely used. Dummy particles were used by Randles & Libersky (1996), ghost particles by Randles & Libersky (1996), Dynamic Boundary conditions by Crespo et al. (2007) and repulsive boundary conditions by Monaghan (1994) and Monaghan (2005). In this paper, the ghost particles method proposed by Randles & Libersky (1996) is used. The ghost particles (see Figure 3) produce a repulsive force when the particles are close to the boundary and the ghost particles are distributed outside the domain and reflected in the boundary. The ghost particle quantities are updated with those of the fluid particles. In this approach, when a fluid particle i becomes close enough to the wall, the ghost particle will be created as a reflection of particle i in the boundary with the following position, velocity, density and pressure:

$$x_{iG} = 2x_{wall} - x_i$$

$$v_{iG} = 2v_{wall} - v_i$$

$$u_{iG} = u_i$$

$$\rho_{iG} = \rho_i$$

$$p_{iG} = p_i$$

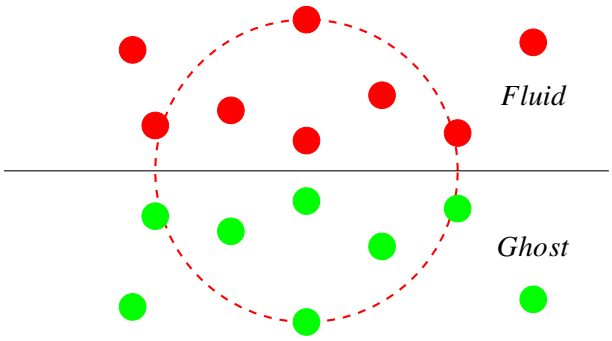

Fig. 3 The implementation of ghost boundary.

Here u and v are the tangential and normal velocity to the wall boundary, respectively.

Moving bodies with SPH

Referring to the figure below, the ghost images of the upper red particles are the particles coloured black. The images of the lower red particles are coloured green. The upper red particles interact only with the black particles, whereas the lower red particles interact only with the green ones. Finally, to move the body itself, here we use the experimental velocity data (Ma et al. (2016)) and interpolate the velocity at each time step.

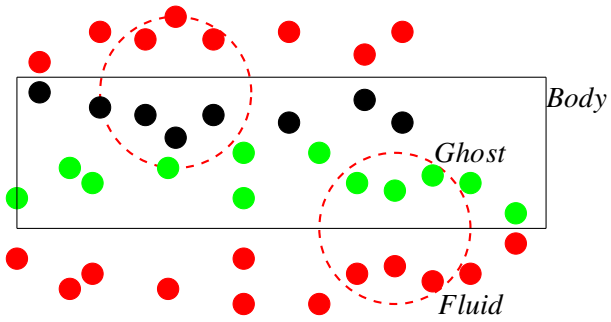

Fig. 4 Schematic of particles close to the body.

Time stepping

In this model, we apply an Euler time stepping scheme. In other SPH simulations such as a dam break and bubble rising through water, we tried the time stepping algorithms such as Verlet and predictor-corrector, but whilst they add complexity, we did not find any significant difference in accuracy in the simulations compared to the Euler scheme. Thus we use Euler here. First, we update the velocity.

$$\boldsymbol{u}_{(t+dt)} = \boldsymbol{u}_{(t)} + \boldsymbol{a}_{(t)} dt,$$

Second, the positions use the results from the velocity update to predict the new position.

$$\boldsymbol{x}_{(t+dt)} = \boldsymbol{x}_{(t)} + \frac{1}{2}(\boldsymbol{u}_{(t)} + \boldsymbol{u}_{(t+dt)})dt.$$

Simulation of 2D impact flat plate

The motion of a flat plate dropping onto water has been investigated experimentally in the FROTH project at Plymouth University. Figure 5 shows the computational set up corresponding to the experimental tests for both pure water and entrained water with air bubbles, Ma et al. (2016). The plate is 0.25 m long and 0.25 m wide, with thickness 0.012 m. The impact velocity is between 4 m/s and 7 m/s, by adjusting the initial position of the flat plate. In our 2D simulation, the pressure has been predicted during impact by evaluating the SPH sum at three points on the plate: at the centre and near the two edges. Flat plate impact calculations are compared with the experimental data for a given initial velocity. On the basis of previous experience gained in performing computations of related free surface flows we use uniformly spaced 600 x 100 particles to discretize the domain. A grid independence study will eventually be required to determine the level of convergence of the results, which must be considered to be indicative only at present. In this study, we set 0.1 m as the initial distance between the flat plate and free surface of the water. The water tank is 6 m long and 1 m depth. Following the Ma et al. (2016), we shifted all time series to correlate first peak pressure at $P1$ to time $t = 0$.

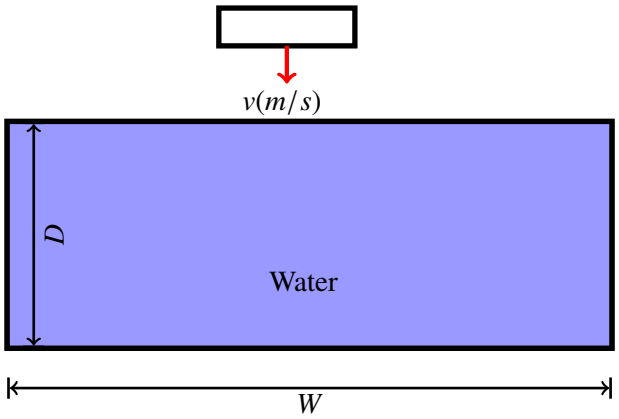

Fig. 5 Schematic representation of impact of a flat plat

Fresh water entry

Firstly the fresh water is considered. Figures 6 and 7 show the comparison of the time series of gauge pressure at the bottom centre of the plate for an impact velocity $v = 4m/s$ and $v = 5m/s$ respectively. The SPH results agree well with experimental results, Ma et al. (2016), and in general, the SPH method and FROTH project at Plymouth University experiments give almost the same pressure evaluation at peak.

Figure 8 shows the pressures are not equally distributed on the plate. The pressure increases from the edge of the flat plate to the centre.

Aerated water entry

In this section, we investigate the effects of aerated water entry on the pressure. The case shown in Figure 5 for pure water, is also used for the aerated water entry. The aeration levels in the water are 0.78%, 1.02% and 1.6%. We use the same number of particles as for pure water entry and again measure the pressure on the bottom of the flat plat at the centre and near the two edges of the plate. The pressures at these three locations are computed by using an SPH sum.

Figure 17 shows the pressure propagation within the water for 0.78% , 1.02% and 1.6% aeration levels at the location centre of the plate. Snap-

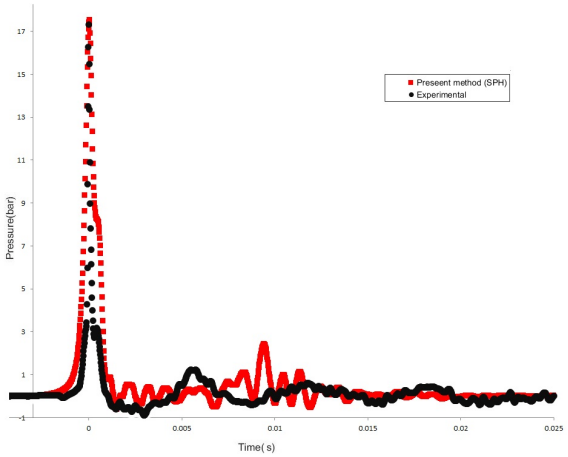

Fig. 6 Pressure-time series for flat plate impact on a fresh water. The impact velocity is 4 m/s

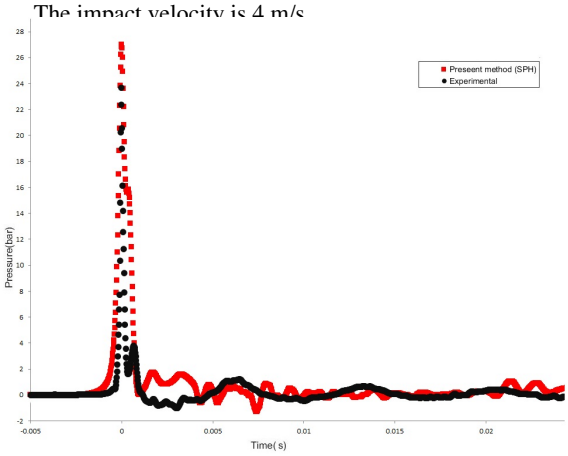

Fig. 7 Pressure-time series for flat plate impact on a fresh water. The impact velocity is 5 m/s

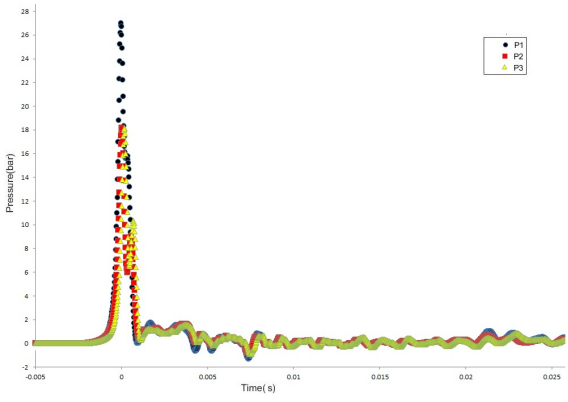

Fig. 8 Pressure distribution on the plate at p_1, p_2 and p_3. The impact velocity is 5 m/s

shots for two cases, 0.78 % and 1.6% aeration level, are presented in figures 9-12 and 13-16. The pressure wave clearly travels faster for the 0.78% aerated level than for the 1.6% level, due to the higher sound speed in the former. At 0.0232s, the pressure wave for 0.78% aeration has reached the tank floor (see figure 11) but in the 1.6% aeration level it has not reached the floor yet (see figure 15).

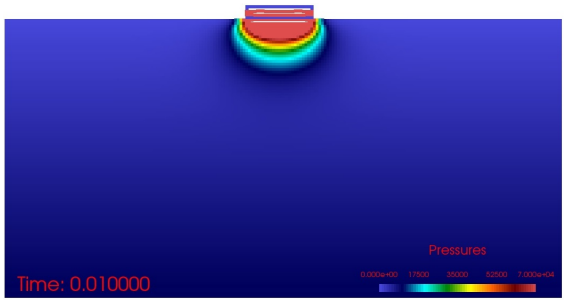

Fig. 9 Snapshot of pressure contour of dropping flat plate into water at t=0.01s, $v = 4m/s$ and aeration level is 0.78%

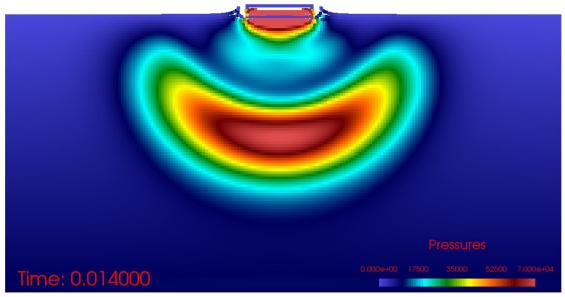

Fig. 10 Snapshot of pressure contour of dropping flat plate into water with aeration 0.78% and $v = 4m/s$ at t=0.019s after impact.

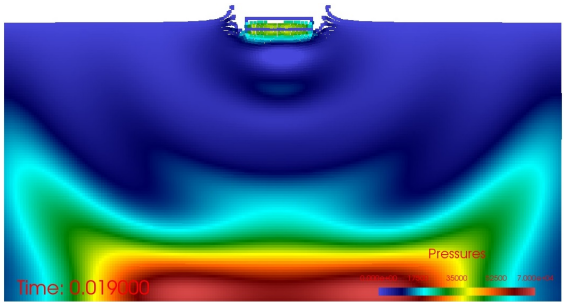

Fig. 11 Reflection of pressure wave after reached the floor of tank at t=0.0232s with aeration 0.78% and $v = 4m/s$

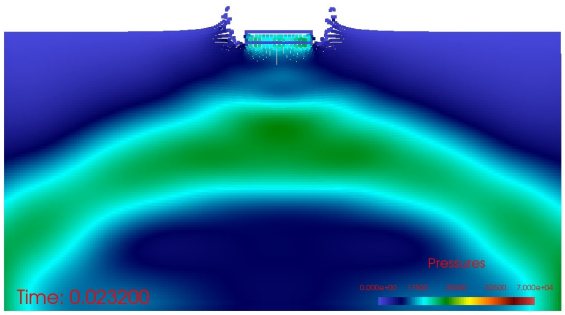

Fig. 12 Predicted water jet flows and pressure contours in water tank at t=0.0338s. with aeration 0.78% and $v = 4m/s$.

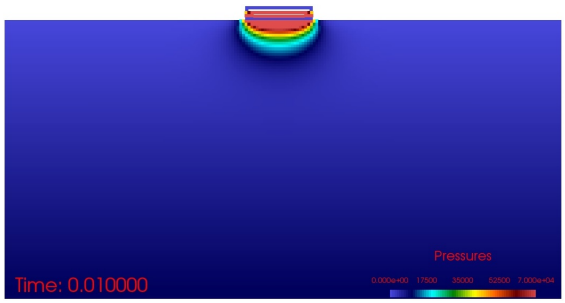

Fig. 13 Snapshot of pressure contour of dropping flat plate into water at t=0.01s, $v = 4m/s$ and aeration level is 1.6%

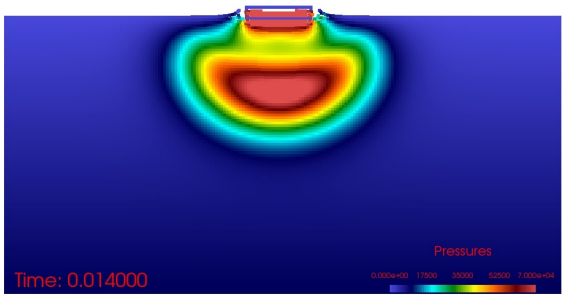

Fig. 14 Snapshot of pressure contour of dropping flat plate into water at t=0.019s after impact, $v = 4m/s$ and aeration level is 1.6%

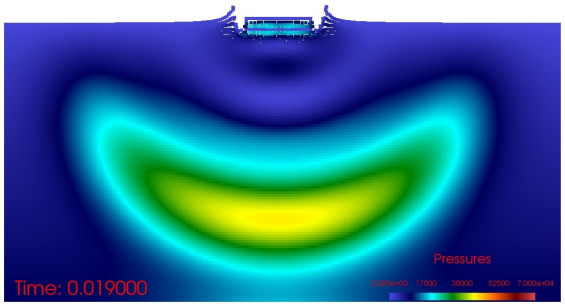

Fig. 15 Reflection of pressure wave after reached the floor of tank at t=0.0232s, $v = 4m/s$ and aeration level is 1.6%

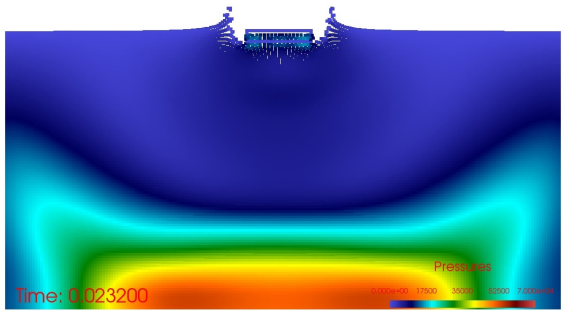

Fig. 16 Predicted water jet flows and pressure contours in water tank at t=0.0338s. $v = 4m/s$ and aeration level is 1.6%

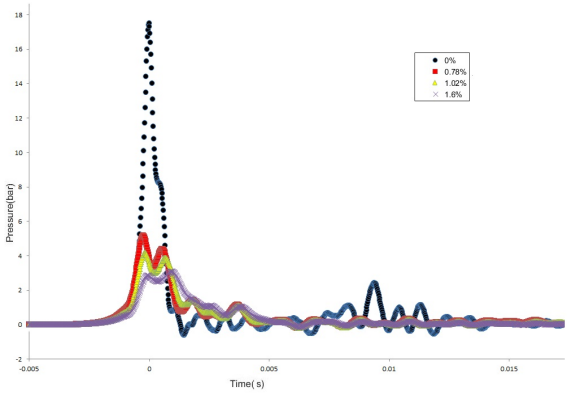

Fig. 17 Pressure-time series for flat plate impact with different aeration levels for $v = 4m/s$

Figures 18, 19 and 20 show that in the experiments, the peak impact pressure on the centre of flat plate is reduced by increasing the aeration level. Simulation results show reasonably good agreement with the experiments. Figure 21 shows the arrangement of pressure sensors on the flat plate.

Table 1 shows the peak pressure values on the flat plate for velocities $4m/s$, $5m/s$ and $7m/s$. For the case with velocity $4m/s$, the maximum value of the peak pressure at P_2 is 17.50 bar for the SPH simulation and 16.98 bar from the experiments. At the both sides P_1 and P_3, the computed pressure at the impact are 12.50 and 12.5 bar whilst the experimental pressures are considerably lower at 6.43 and 5.23 bar, respectively. Tables 2, 3 and 4 list all peak loading pressures on the plate at different locations, with velocities $4m/s$, $5m/s$ and $7m/s$ for experimental results and SPH simulations.

Table 5 shows a comparison between experimental and numerical values of the pressure impulse evaluated at points P1, P2 and P3 for the unaerated water impact at 4ms^{-1}. The pressure impulse is defined as the time integral of the pressure over the duration of an impact event. Again the comparison is good. Note that the pressure impulse is approximated here as

$$I = \frac{1}{2} P_{max}(\delta t_{up} + \delta t_{dn})$$

where P_{max} is the maximum impact pressure and (δt_{up} and δt_{dn} are the rise and fall times of the maximum pressure.

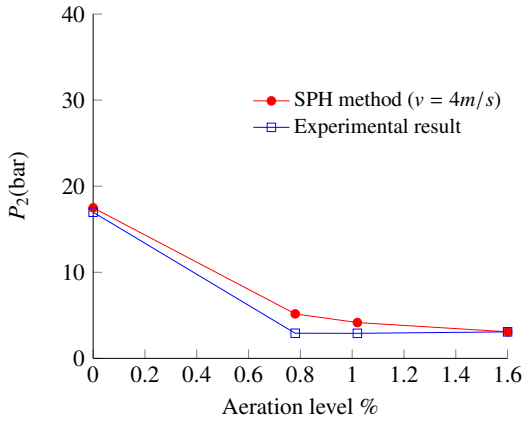

Fig. 18 The peak impact gauge pressure affected by aeration at $v = 4m/s$

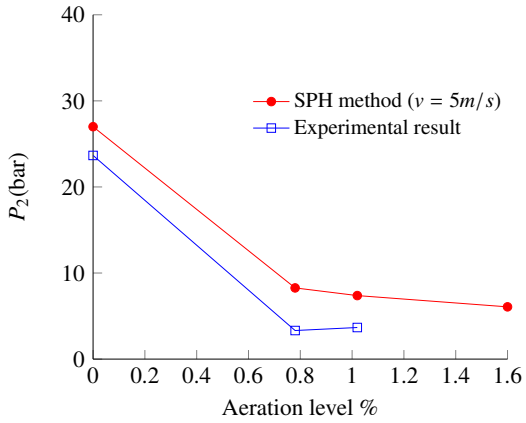

Fig. 19 The peak impact gauge pressure affected by aeration at $v = 5m/s$

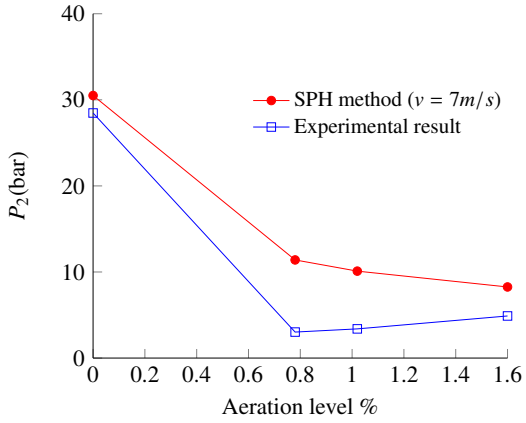

Fig. 20 The peak impact gauge pressure affected by aeration at $v = 7m/s$

	$v = 4m/s$		$v = 5m/s$		$v = 7m/s$	
	Experimental	SPH	Experimental	SPH	Experimental	SPH
P_1	6.43	12.50	7.766	20.50	15.286	18.60
P_2	16.98	17.50	23.66	27	28.47	30.50
P_3	5.23	12.50	10.713	20.50	18.39	18.60

Table 1 Maximum gauge pressure of the plate with aeration level=0%

3D FLAT PLATE DROPPING

The computational setup is similar to that used in the previous section. A 25cm x 25cm flat plat is dropped at a specified velocity onto a still water surface. Fluid particles are distributed uniformly and the number of particles used in this simulation is 768000, with particle spacing $dx = dy = dz = 0.01$, where dx, dy and dz are the initial particle distances. The numbers of particles in the x, y and z-directions are 160, 160 and 30 particles, respectively. After 0.01s the plate collides with the free surface. Pressures are again calculated during the simulation at these 5 points using an SPH sum. From Figure 22, Figure 23 and 24, we can see the developing splash created by the impact.

Figure 25, 26 and 27 show much larger pressures at the centre of the plate and essentially symmetrical values at the edges.

	$v = 4m/s$		$v = 5m/s$		$v = 7m/s$	
	Experimental	SPH	Experimental	SPH	Experimental	SPH
P_1	3.898	3.51	6.087	5.57	2.923	7.37
P_2	2.92	5.17	3.32	8.27	3.02	11.40
P_3	3.825	3.51	3.943	5.56	8.360	7.37

Table 2 Maximum gauge pressure of the plate with aeration level=0.78%

	$v = 4m/s$		$v = 5m/s$		$v = 7m/s$	
	Experimental	SPH	Experimental	SPH	Experimental	SPH
P_1	4.22	2.80	4.127	4.66	6.1445	6.28
P_2	2.91	4.16	3.67	7.38	3.39	10.10
P_3	2.83	2.80	4.032	4.77	6.18604	6.51

Table 3 Maximum gauge pressure of the plate with aeration level=1.02%

	$v = 4m/s$		$v = 5m/s$		$v = 7m/s$	
	Experimental	SPH	Experimental	SPH	Experimental	SPH
P_1	2.903	1.9	–	3.84	6.5809	5.22
P_2	3.08	3.09	–	6.07	4.89	8.26
P_3	2.894	1.96	–	3.96	5.87	5.35

Table 4 Maximum gauge pressure of the plate with aeration level=1.6%

	$v = 4m/s$		$v = 5m/s$		$v = 7m/s$	
	Experimental	SPH	Experimental	SPH	Experimental	SPH
P_1(Pa s)	225	215	719.71	709	851.03	894
P_2(Pa s)	207	166	359	572	487.58	560
P_3(Pa s)	130.01	169	388	575	514	568

Table 5 Pressure impulses of impact on the plate for pure water entry 0% is calculated before and after shock

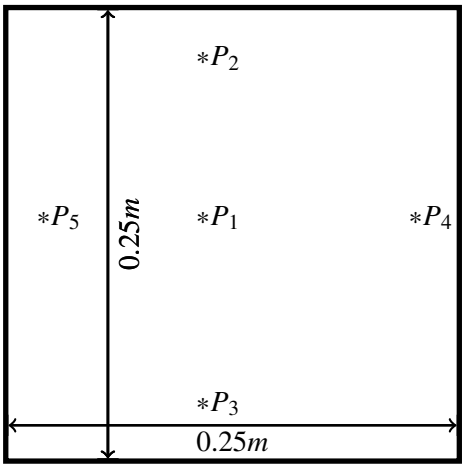

Fig. 21 Schematic representation of 3D of a flat plat

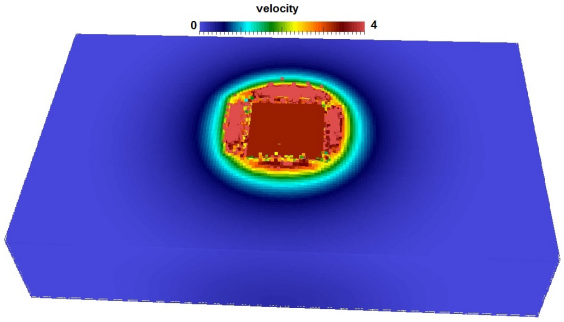

Fig. 22 Snapshot of dropping flat plate into initially still water at t=0.01s viewing from above.

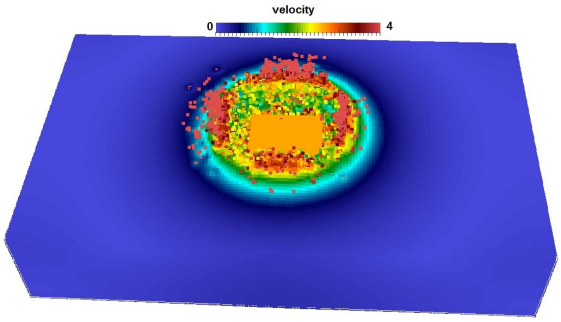

Fig. 23 Snapshot of dropping flat plate into initially still water at t=0.0196s viewing from above

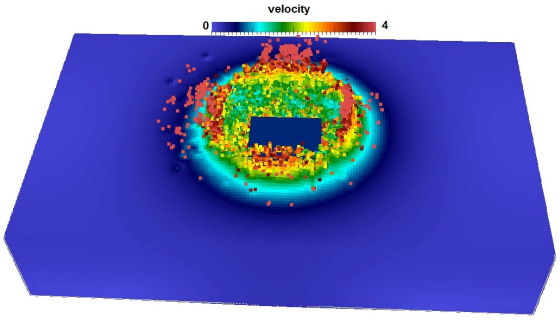

Fig. 24 Snapshot of dropping flat plate into initially still water at t=0.038s viewing from above.

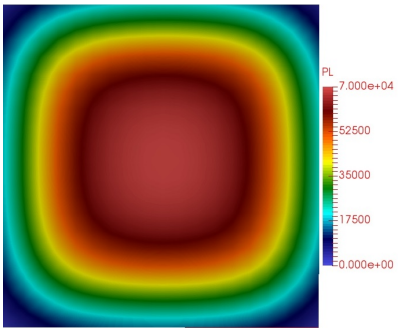

Fig. 25 Pressure contours distribution on the plate at $t = 0.01s$.

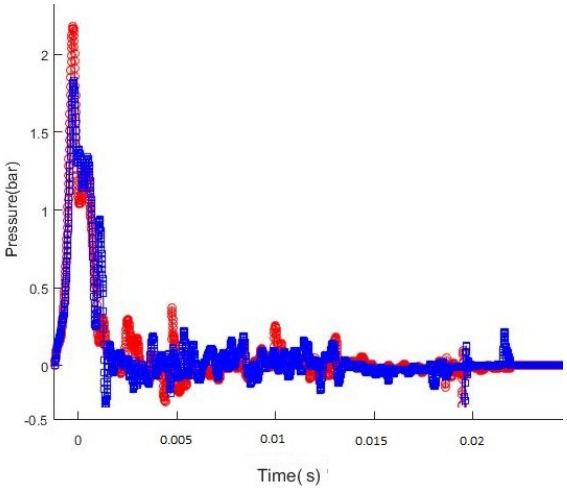

Fig. 26 Pressure distribution on the plate at p_2, p_3.

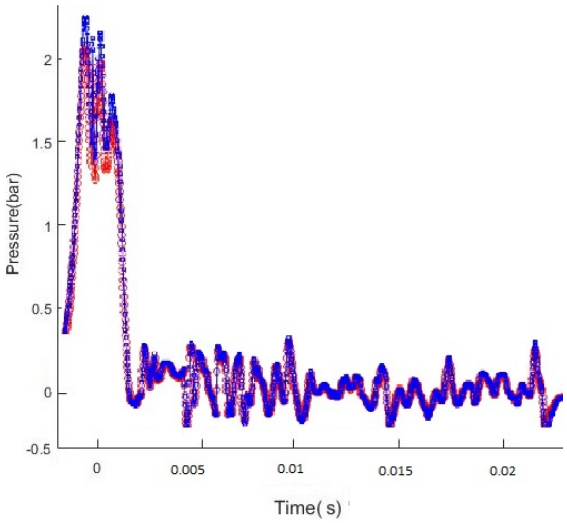

Fig. 27 Pressure distribution on the plate at p_4, p_5.

CONCLUSIONS

In this paper, we used the SPH method to simulate a flat plat impacting on a water surface with different water aeration levels and at different impact speeds. The preliminary results shown here indicate that the computed impact loading on the flat plate during the water entry is in generally good agreement with the experimental results. The numerical and experimental results show the pressure peak on the plate will be reduced from 30.5 bar in pure water to 8.25 bar in water aerated with 1.6% air. In the future, we will investigate 2D and 3D multiphase simulations of the flat plate impact.

References

Brennen, C. E. (1995), *Cavitation and Bubble Dynamics*, Oxford University Press, Oxford, chapter 6.

Crespo, A., Gómez-Gesteira, M. & Dalrymple, R. A. (2007), 'Boundary conditions generated by dynamic particles in sph methods', *CMC-TECH SCIENCE PRESS-* **5**(3), 173.

Gingold, R. A. & Monaghan, J. J. (1977), 'Smoothed particle hydrodynamics: theory and application to non-spherical stars', *Monthly notices of the royal astronomical society* **181**(3), 375–389.

Lucy, L. B. (1977), 'A numerical approach to the testing of the fission hypothesis', *The astronomical journal* **82**, 1013–1024.

Ma, Z., Causon, D., Qian, L., Mingham, C., Mai, T., Greaves, D. & Raby, A. (2016), 'Pure and aerated water entry of a flat plate', *Physics of Fluids* **28**(1), 016104.

Monaghan, J. (1994), 'Simulating free surface flows with {SPH}', *Journal of Computational Physics* **110**(2), 399 – 406.

Monaghan, J. J. (2005), 'Smoothed particle hydrodynamics', *Reports on Progress in Physics* **68**(8), 1703.
URL: *http://stacks.iop.org/0034-4885/68/i=8/a=R01*

Morris, J. P., Fox, P. J. & Zhu, Y. (1997), 'Modeling low reynolds number incompressible flows using sph', *J. Comput. Phys.* **136**(1), 214–226.

Panizzo, A. & Dalrymple, R. (2004), 'Sph modelling of underwater landslide generated waves', *COASTAL ENGINEERING CONFERENCE* **29**, 1147.

Randles, P. & Libersky, L. (1996), 'Smoothed particle hydrodynamics: Some recent improvements and applications', *Computer Methods in Applied Mechanics and Engineering* **139**(14), 375 – 408.
URL: *//www.sciencedirect.com/science/article/pii/S0045782596010900*

Wendland, H. (1995), 'Piecewise polynomial, positive definite and compactly supported radial functions of minimal degree', *Advances in computational Mathematics* **4**(1), 389–396.